The influence of macrofaunal burrow spacing and diffusive scaling on sedimentary nitrification and denitrification: An experimental simulation and model approach

Franck Gilbert, Robert Curwood Aller, Stefan Hulth

The influence of macrofaunal burrow spacing and diffusive scaling on sedimentary nitrification and denitrification: An experimental simulation and model approach

by Franck Gilbert[1], Robert C. Aller[2] and Stefan Hulth[3]

ABSTRACT

The influence of burrow spacing on sedimentary nitrification and denitrification was simulated experimentally using sediment plugs of different thicknesses immersed in aerated seawater reservoirs. Different plug thicknesses mimic different distances between oxygenated burrow centers and produce similar changes in aerobic–anaerobic reaction balances as a function of diffusive transport scaling. The thicknesses used were roughly equivalent to transport scales (interburrow spacing) that could be produced by burrow abundances of $\sim$400 to 50,000 m^{-2}, depending on burrow lumen radii (e.g., 0.05–1 cm). Following the exposure of anoxic sediment plugs to aerated water, an efficient aerobic nitrification zone was established within the first $\sim$2–3 millimeters of sediment. At pseudo-steady state, the thinnest plug (2 mm) simulating highest burrow density, was entirely oxic and the denitrification rate nil. Denitrification was stimulated in anoxic regions of the thicker plugs (5, 10, and 20 mm) compared to the initial value in experimental sediment. Maximum nitrification rates and the highest denitrification/nitrification ratio between oxic nitrification and adjacent denitrification zones occurred for the intermediate plug thickness of 5 mm. Of the oxic/anoxic composites, the thickest plug showed the least efficient coupling between nitrification/denitrification zones (lowest denitrification/nitrification ratio). Both the thickness of the oxic layer and the total net remineralization of dissolved inorganic N varied inversely with plug thickness. A set of diffusion–reaction models was formulated assuming a range of possible nitrification kinetic functions. All model forms predicted optimal nitrification–denitrification and ammonification–denitrification coupling with relative oxic–anoxic zonation scales comparable to intermediate plug thicknesses (5–6 mm). However, none of the commonly assumed kinetic forms for nitrification could produce the observed NO$_3^-$ profiles in detail, implying that natural sediment populations of nitrifiers may be less sensitive to O$_2$ than laboratory strains. Our experimental and model results clearly show that rates of N remineralization and the balance between stimulation/inhibition of denitrification are highly dependent on sedimentary biogenic structure and the particular geometries of irrigated burrow distributions.

1. Laboratoire d'Océanographie et de Biogéochimie (COM), UMR CNRS 6535, Faculté de Luminy, Case 901, F-13288 Marseille Cedex 9, France. *e-mail: gilbert@com.univ-mrs.fr*
2. Marine Sciences Research Center, State University of New York at Stony Brook, Stony Brook, New York, 11794-5000, U.S.A.
3. Analytical and Marine Chemistry, Göteborg University, SE-41296 Göteborg, Sweden.

1. Introduction

Sedimentary denitrification is one of the major components of the marine nitrogen cycle (e.g. Seitzinger, 1988; Seitzinger and Giblin, 1996). Denitrification consumes dissolved nitrate, remineralizes C_{org}, and exports gaseous nitrogen to the atmosphere (Knowles, 1982). Although an anaerobic process, denitrification has an antipodal interaction with O_2 in sediments. Oxygen inhibits the enzymes of denitrification (Firestone *et al.,* 1980) but also stimulates sedimentary nitrification which usually provides the major source of NO_3^- for denitrification (Billen, 1982). Bioturbation of sedimentary deposits typically generates close juxtapositions of oxic and anoxic microenvironments around biogenic structures and strongly influences both nitrification and denitrification. There is often a general stimulatory effect of macrobenthic activity, and particularly bioirrigation, on sedimentary nitrification and denitrification (Sayama and Kurihara, 1983; Kristensen and Blackburn, 1987; Henriksen and Kemp, 1988; Pelegri *et al.,* 1994; Mayer *et al.,* 1995; Rysgaard *et al.,* 1995; Gilbert *et al.,* 1998). Field measurements have demonstrated that denitrification rates can also vary inversely with bioirrigation intensity at the highest irrigation rates (Berelson *et al.,* 1998). Direct comparison of the causes and magnitudes of reported stimulation (from 114 to 950%) or inhibition is virtually impossible because both the macrofaunal species and the organism abundances are distinct to each study. Species-specific burrow properties such as mucous secretions, burrow wall construction, or irrigation behavior are known to affect nitrification and denitrification, and require characterization of individual species (Aller *et al.,* 1983; Kristensen *et al.,* 1985, 1991; Mayer *et al.,* 1995). In contrast, the likely effects of population abundance or burrow spacing, and the corresponding changes in transport-reaction structure, can in principle be isolated by geometrically simulating variations in the distances between burrows.

A primary effect of irrigated tubes or burrows is to create diffusive sources or sinks for pore water solutes within otherwise isolated portions of sedimentary deposits. Stagnant burrows have no discernable effects on pore water distributions, and frequent irrigation is required to maintain local oxygenated conditions and diffusive concentration gradients between burrow lumen and surrounding sediment pore water (Aller, 1984; Kristensen, 1988; Boudreau and Marinelli, 1994). In order to examine the general impacts of irrigated burrows and the associated macro-transport structure on nitrification and denitrification independently of species-specific effects, we carried out an experiment in which plugs filled with sediment were exposed continuously to oxygenated overlying water (e.g. Aller and Mackin, 1989). Our experimental design was based on the concept that the characteristic scales of diffusion, and thus transport–reaction patterns within the bioturbated zone of muddy deposits, are determined in large part by the time-averages of size and effective spacing of irrigated burrow structures (Aller, 2001). By simply varying plug thickness (L; Fig. 1A), we simulated different spacings between irrigated burrows and the resulting degrees of sediment oxygenation, thereby altering the relative extent of coupled nitrification and denitrification zones, and mimicking changes in burrow density (Aller and Aller, 1998; Hulth *et al.,* 1999).

Our experimental setup allowed us to simulate a wide range of effective burrow
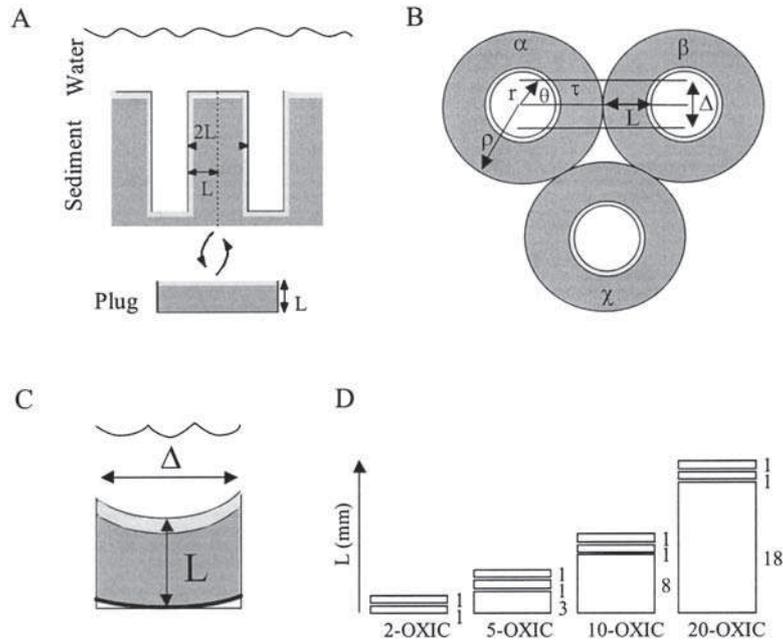
Figure 1. (A) Schematic diagram of two idealized, identical burrow structures shown separated in the axial plane at a particular time by a constant characteristic distance $2L$. Light areas indicate oxygenated zones, dark are anoxic. In reality, the distance $2L$ and axial orientation vary as a complex function of space and time, however, the basic physical interactions between irrigation centers are represented in the idealized geometry. (B) Idealized view perpendicular to axis of hexa-net packed burrows or burrow structure microenvironments (α, β, χ) having burrow lumen radius r. In this case the orientation of the plane is parallel to the sediment surface in (A) but may be thought as having an arbitrary orientation within a sedimentary deposit. Because sedimentary solutes must achieve a concentration minimum or maximum at distance $\sim L$ (no net flux) between identical structures, a characteristic diffusion scale $L = (\rho - r)$ can be considered along the segment τ between any two burrow centers. This diffusive scaling within the plane applies roughly to the swath of sediment $\Delta = 2r \sin(\theta)$ with a fractional variation around L of $\sim r(1 - \cos(\theta))/(\rho - r)$. Because irrigated microenvironments are never exactly identical, the scaling L may lie away from the midpoint between any two burrow centers. (C) The effect of variable interburrow spacing on the characteristic diffusion scale (L) can be simulated approximately by sections of planar sediment exposed on one surface and with sealed bottoms (i.e., no net flux basal condition). The scale Δ is not critical to examining the effect of scale L per se but is an indication of spatial extent over which a given approximation applies (smaller as $r/\rho \to 0$). The planar diffusion and one dimensional scale approximation to radial diffusion distributions becomes most accurate as $r/\rho \to 1$. (D) Different thicknesses (lengths) of plugs were used in the present experiments to mimic different time-averaged burrow spacings which might occur at various locations within bioturbated sediments (L values are expressed in millimeters). The upper 2 mm of plugs were divided at 1 mm intervals by use of stacked rings of 1 mm thickness, allowing rapid accurate sectioning at time of sampling.

abundances from medium ($\sim$400 m^{-2}) to high density ($\sim$50,000 m^{-2}, e.g., Ronan, 1978; Aller *et al.,* 2002), depending on the exact burrow lumen radii (e.g., 0.05–1 cm). A characteristic diffusive transport scale L resulting from a particular burrow abundance is given approximately by ($\rho - r$), where $\rho \sim 1/\sqrt{\pi N}$ (N = burrow abundance per area) and r = radius of the irrigated burrow center or lumen (Fig. 1). The use of a planar transport geometry in our experimental manipulations does not exactly mimic the radial or irregular diffusive coupling between reaction zones typically found around burrows or between sectors of individual burrows, but it is sufficient to demonstrate the basic principles involved (Fig. 1).

2. Materials and methods

a. Experimental procedure

Surface (0–2 cm) muddy sediment and overlying seawater were collected using a Ponar grab at station P ($\sim$14 m) in central Long Island Sound, USA, during June 1997 (see: Gérino *et al.,* 1998; for station P description; salinity 24–28, silt-clay, $\sim$2% organic C, $\sim$3% CaCO$_3$). All materials used in the laboratory for sampling, storage and chemical analyses were precleaned with HCl and rinsed with double distilled water and seawater. Experimental containers for holding sediment were made of sections of PVC pipes cut into rings (two diameter sizes: small, 2.1 cm ID; large, 5.2 cm ID). First, 1, 3, 8 and 18 mm length PVC rings were fixed on individual circular PVC base sheets. Then, one or two additional 1 mm thick rings were stacked on the basal rings in order to obtain 4 groups of sediment plugs having total thicknesses (lengths) of: 2, 5, 10 and 20 mm (Fig. 1B). A second group of polycarbonate plug containers (2.85 cm ID) of equivalent total thicknesses (lengths) was used for the measurement of denitrification activity only.

All plugs were filled with sediment that had been sieved through a 0.5 mm nylon mesh (no added water) to remove macrofauna and homogenized by hand stirring under N$_2$ in a glove bag. Sets of plugs having the same thickness (single set = 9 large PVC plugs, 1 small PVC plug and 4 polycarbonate plugs; Fig. 2), were then submersed in large polycarbonate reservoirs containing 15.4 l of 0.2-μm filtered seawater continuously purged with water-saturated air. These plug sets were termed 2-OXIC, 5-OXIC, 10-OXIC, 20-OXIC respectively, depending on thickness (2-, 5-, 10-, 20-mm). As a control, another reservoir without sediment plugs (BLANK) was also filled with filtered and aerated seawater. Subsamples of the experimental sediment were dried to constant weight at 60°C for determination of saturated porosity.

Water reservoirs were continuously stirred by a centrally located magnetic stir bar at a rate slightly below that necessary to suspend sediment (in order to minimize diffusive boundary layers). Overlying water ($\sim$20 ml) from each container was periodically sampled (after 0, 1, 3, 5, 7, 9 and 13 days) with a syringe and analyzed. After 13 days, plugs were removed from reservoirs, sediment layers were sliced by sliding off individual rings of a stack, placing the sediment into plastic syringes, and porewater separated from the sediment (large plugs) by squeezing in individual syringe presses. There was no discern-
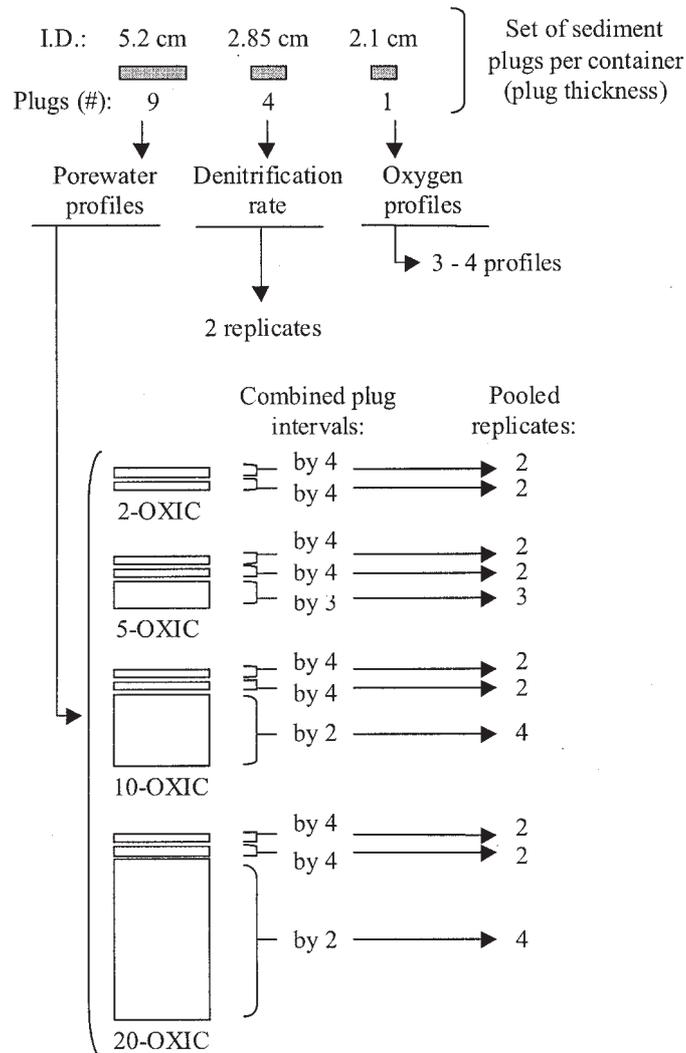
Figure 2. Schematic diagram of experimental setup. Inner diameters (I.D.) and numbers of plugs used for the different measurements are indicated. Each container held a complete set of plugs having a single overall thickness (14 plugs). The depth interval sampling scheme for pore water is shown for each type of plug of a given overall thickness. The equivalent depth intervals from several plugs having the same total thickness were combined into single samples for pooled analysis. For example, the top 0–1 mm of sediment from 4 separate plugs in the 2 mm thick plug container was combined into a single pooled sample. There were 2 such combined samples (composed of 4 plugs each) representing the sampling of pore water from 8 plugs overall.

able compaction or expansion of sediment relative to starting thicknesses within individual plugs. Pore water sampling and separations were completed within several minutes following removal of individual plugs from water reservoirs. Pore water from particular

depth intervals in multiple plugs of the same length were combined as necessary to obtain sufficient sample for analyses, resulting in 2 pooled replicates for each of the 1 mm intervals and up to 4 replicates for the thicker basal sections (Fig. 2).

b. Chemical analyses: denitrification

Denitrification rates were assessed using the acetylene-blockage method. Sediment subsamples (0.7 ml for the 2-mm thick plugs, 1 ml for the others) from duplicate polycarbonate plugs were transferred into 5 ml tubes with 2 ml of seawater from each corresponding reservoir. Seawater was supplemented with chloramphenicol (final concentration: $1 \, g \, L^{-1}$) to prevent new bacterial growth during incubation and to extend the period of linear N_2O accumulation (Tiedje *et al.,* 1989). The tubes were sealed with rubber stoppers and anaerobic conditions were obtained by flushing N_2 through the tube for 2 min. Acetylene, which inhibits the reduction of N_2O to N_2 (Balderston *et al.,* 1976), was injected in the gas phase (final pressure: 15 kPa) and the tubes were vortexed. Samples were incubated in the dark at experimental temperature for 0, 1, 3, 5 and 8 h. After incubation, each tube was fixed with 0.1 ml of 1 M $HgCl_2$ solution to terminate reaction.

Nitrous oxide in the tubes was determined by gas chromatography (HP5890, Series II) using an electron capture detector and an automatic injector (Dani HSS 86.50). The nitrous oxide detection limit was 100 nM. Chromatographic operating conditions: oven temperature: 50°C; injector temperature: 150°C; detector temperature: 260°C. Nitrogen was used as carrier gas (20 ml min^{-1}) for the ECD GC system.

c. Chemical analyses: oxygen, nutrients

The smaller PVC plugs were used for the determination of oxygen distribution using a Clark-style combination microelectrode (Revsbech *et al.,* 1980). The electrode was standardized in seawater saturated with air or nitrogen at 22°C, and the zero value also checked by insertion of the electrode deep into a separate container of anoxic sediment. A gas exchange FIA-technique using conductivity detection as described by Hall and Aller (1992) was used to determine ammonium concentrations. Concentrations of nitrite and nitrate were determined using standard colorimetric methods (Strickland and Parsons, 1972) applied to a miniaturized flow injection system. Analytical precisions were generally ~2–5% SD and less than variability between plug samples.

3. Results

a. Overlying water N-compound changes with time

N-compound concentrations changed regularly both in magnitude and speciation as a function of time in the different overlying water reservoirs (Fig. 3). Reservoirs were continuously aerated and stirred. The basic relative patterns of DIN (NH_4^+, NO_2^-, NO_3^-) in each reservoir were the same. These relative changes consisted of an initial release and rapid buildup of NH_4^+, followed by progressive oxidation and successive conversion to NO_2^- and NO_3^-, and then a continued, but slowed buildup of total DIN, largely as NO_3^-,

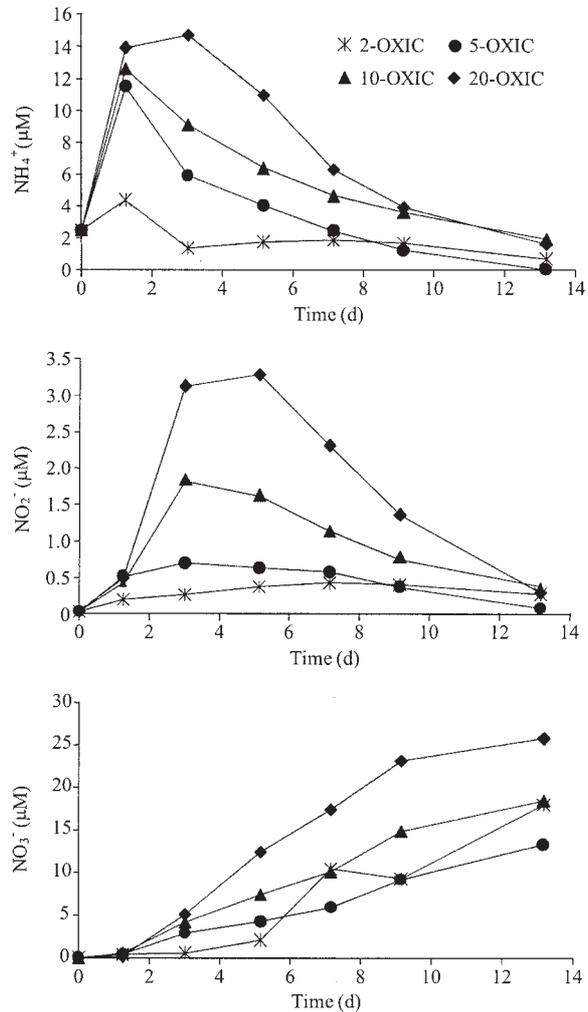Figure 3. Nitrogen compound (NH_4^+, NO_2^- and NO_3^-) concentrations as a function of time in overlying water reservoirs for the different sediment plug thicknesses.

over the remainder of the experiment. The magnitude of DIN concentrations obtained in each case depended directly on the quantity of sediment present in the reservoir, i.e. plug thickness (Fig. 3). These general patterns are typical of the classically recognized successions of DIN speciation observed during remineralization (ammonification) and nitrification.

In detail: following initial exposure of oxygenated water to anoxic sediment plugs, NH_4^+ concentrations increased sharply until the second day, reaching maxima of 4.38 to 13.90 μM for 2-OXIC and 20-OXIC respectively, and then decreased exponentially to final concentrations after 13 days of <0.04 (detection limit) to 1.94 μM, all lower than the

Table 1. Concentrations in the sediment and overlying water and sediment denitrification rate prior to the open plug incubations (mean, $n = 2$).

	$\Sigma NO_3^- + NO_2^-$ (μM)	NO_2^- (μM)	NH_4^+ (μM)	Denitrification rate (μmol $N_2O\ L^{-1}\ d^{-1}$)
Porewater	1.5	0.6	640	37.7
Overlying water	0.0	0.03	2.5	—

starting value (2.5 μM; Table 1). Although total DIN continued to increase in the overlying water over time, the initially released NH_4^+ pools were progressively oxidized first to NO_2^- and then NO_3^-, with the intermediate NO_2^- showing maximum concentrations during the initial stages of conversion (approximately three days). Final concentrations ranged between 0.03 μM (initial concentration; Table 1) and 0.5 μM. NO_3^- concentrations were quite stable the first day and then continuously increased to reach final concentrations from 13.45 μM (5-OXIC) to 26.08 μM (20-OXIC) (Fig. 3). In the control container without sediment (BLANK), final concentrations were 1.02, 0.4 and 4.01 μM for NH_4^+, NO_2^-, and NO_3^-, respectively.

b. Oxygen penetration patterns

Oxygen progressively diffused into the initially anoxic sediment plugs and reached pseudo-steady state penetration depths. After the 13 d incubation, O_2 profiles in the sediments showed typical diffusive patterns with the O_2 penetration decreasing inversely with increasing sediment thickness (mean of 3–4 individual profiles) (Fig. 4A). For example, the O_2 concentration at 2 mm depth was 152, 54, 28 and 19 μM for 2-OXIC, 5-OXIC, 10-OXIC and 20-OXIC, respectively.

c. Sedimentary DIN-compound profiles

The sediment in all plugs was initially homogenized and had identical, vertically constant concentrations of NH_4^+, NO_2^-, and NO_3^- (Table 1). These initial concentration profiles changed rapidly following continuous exposure to oxygenated water. Oxic and anoxic sediment zones were established, the relative scales of which depended on total sediment thickness. In contrast to the 2 mm plugs, the partial penetration of O_2 in the cases of the 5, 10, and 20 mm plug sets resulted in varying relative thicknesses of oxic and anoxic redox zones (Fig. 4B). At the time of final sampling, all N reaction patterns and corresponding concentration distributions were expected to be at a pseudo-steady state (see subsequent model calculations). The 2 mm plug set was completely oxidized, and the DIN vertical distributions were characterized by low NH_4^+ and high NO_3^- concentrations, reflecting net nitrification throughout the entire plug and a net NO_3^- flux to the overlying water (Fig. 5).

The surface of each of the thicker plug sets was clearly dominated by nitrification, as indicated by maximum NO_3^- concentrations in either the upper 1 or 2 mm (Fig. 5). These NO_3^- concentrations exceeded overlying water concentrations, demonstrating a diffusive
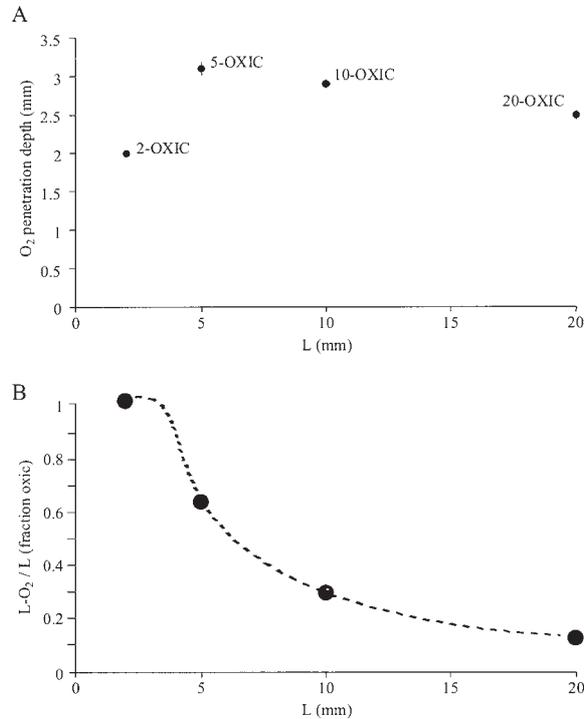
Figure 4. (A) Measured O_2 penetration depth (mean $\pm$ SD) and (B) fraction of total plug thickness that is oxic as a function of plug thickness (L) (dotted line represents interpretive pattern).

flux of NO_3^- into overlying water. Basal anoxic sediment zones had lower NO_3^- concentrations than overlying oxic zones, indicating downward diffusion of NO_3^- and net denitrification. NH_4^+ profiles demonstrated buildup at the bases of each plug set and obvious depletion in the surface 1–2 mm, mirroring surficial NO_3^- increases. Averaged NH_4^+ concentrations in plugs were all lower than the initial pore water NH_4^+ concentration, consistent with both diffusive loss of NH_4^+ to overlying water during transient equilibration conditions (Fig. 3), and also with the consumption of NH_4^+ in the oxic zone during sedimentary nitrification. The profiles of NH_4^+ concentration varied regularly with plug thickness (length), attaining the least overall concentrations in the 2 mm plug set and highest in the basal regions of the 20 mm plugs.

d. Direct measures of sediment denitrification rates

Directly measured denitrification rates showed differences with the plug thickness (Fig. 6). The rate measured in the thinnest, completely oxic plug (less than 0.5 μmol. N_2O L^{-1} d^{-1}) showed a decrease with respect to the initial homogenized sediment rate (37.7 μmol. N_2O L^{-1} d^{-1}, immediately following homogenization). In the remaining plug sediments, denitrification rates in the anoxic zone were increased $\sim$4 to 10 times the initial bulk value (Table 1).
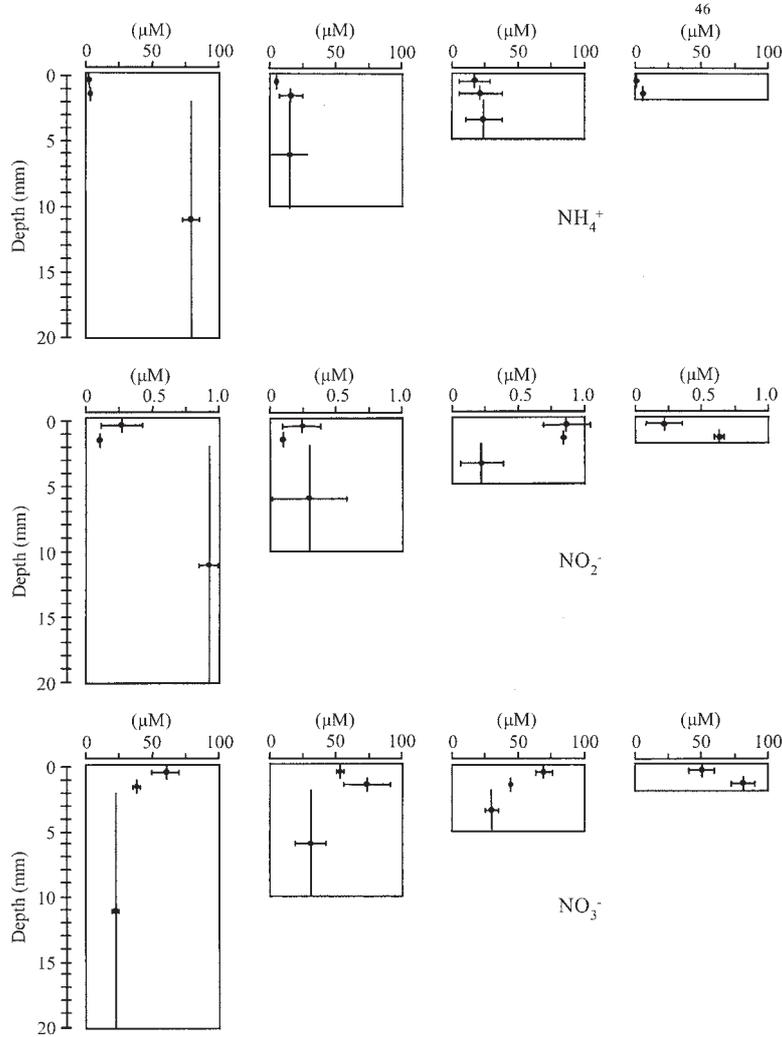
Figure 5. Nitrogen compound concentration (mean $\pm$ SD) profiles in the different sediment plugs at the end of experimentation. Top: NH_4^+, middle: NO_2^-, and bottom: NO_3^-. For the 0–1 and 1–2 mm layers, $n = 2$, for the 2–5 mm layer, $n = 3$, and for the 2–10 and 2–20 mm layers, $n = 4$.

e. Mass balance estimates of N remineralization

Minimum estimates of total net N remineralization rates in the individual plug sets can be obtained from the change between the total mass of DIN present initially and that present at the end of the experiment in each plug set microcosm. Losses of N by denitrification, formation of dissolved organic N during decomposition, or transient uptake into biomass in this case are ignored. The minimum rate of dissolved N production (R_N), assumed equivalent to the ammonification rate over a time interval Δt, is:

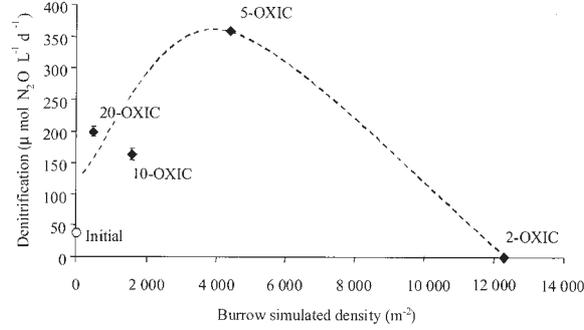$$R_N = [(N_{ow}(\Delta t) + N_{pw}(\Delta t)) - (N_{ow}(0) + N_{pw}(0))]/V_{pw}\Delta t \qquad (1a)$$

Figure 6. Denitrification rate (mean values ± minima and maxima) in the different sediment plugs expressed as a function of the simulated burrow density. The illustrative calculation of the burrow density as a function of the plug thickness (L) was made using an arbitrary internal burrow radius of 5 mm. Dotted curve represents interpretive pattern.

$$N_{ow}(t) = C_{ow}(t) V_{ow} \tag{1b}$$

$$N_{pw}(t) = C_{pw}(t)(1 + K) V_{pw} \tag{1c}$$

Where: $N_{ow}(t)$ = moles of DIN in overlying water at time t
$N_{pw}(t)$ = moles of DIN in pore water or reversibly adsorbed at time t
$C_{ow}(t)$ = concentration of DIN in overlying water at time t
$C_{pw}(t)$ = concentration of DIN in pore water at time t
V_{ow} = volume of overlying water (15.4 l)
V_{pw} = volume of pore water

The concentrations of DIN were summed over NH_4^+, NO_2^-, and NO_3^- measured in overlying water (Fig. 3) and in plugs (averages used; Fig. 5) at the beginning and end of the experiment. Ammonium pore water concentrations were multiplied by the factor $(1 + K)$, where K = reversible adsorption coefficient (dimensionless) to account for adsorption equilibrium with sediment particles. The volume of pore water for each plug set was estimated from the total plug surface exposed (224 cm^2) in each microcosm, plug set thickness, and measured sediment porosity (porosity, $\varphi = 0.774$, assuming particle density of 2.6 g cm^{-3}). The ammonium adsorption coefficient is $K^* = 1.21$ cm^3 g^{-1} (NH_4^+ displacement by 2 N KCl) for the experimental sediment, giving a $K = 0.91$ (Green *et al.,* 1998). The resulting minimum net N production estimates relative to pore water volume are: 616, 79, 47, and 7.3 μM d^{-1} for 2 mm, 5 mm, 10 mm, and 20 mm thick plugs respectively when averaged over the course of the experiment.

f. Diffusive flux estimates of reaction rates

Minimum estimates of diffusive fluxes, J_{diff}, of NO_3^- within sediment plugs and between sediment and overlying water can be made using Fick's first law (Berner, 1980):
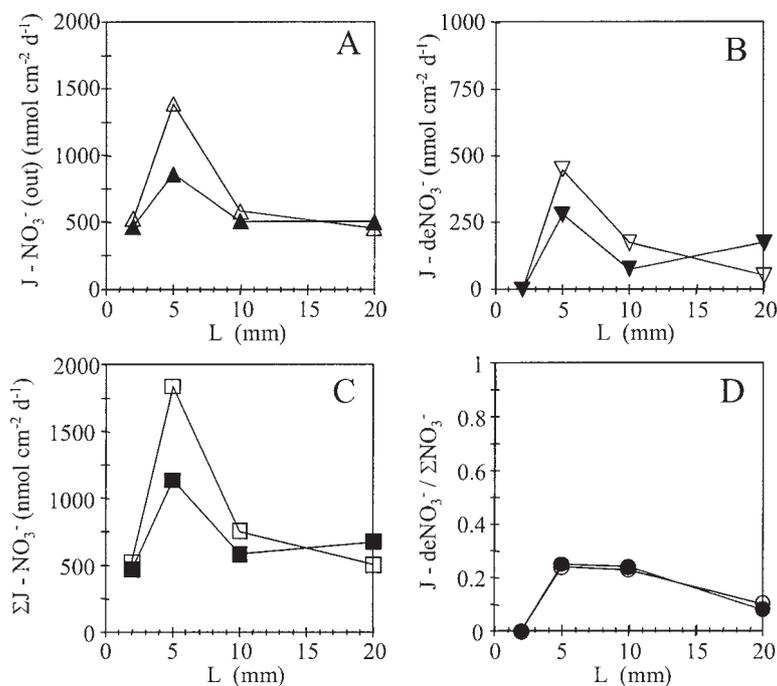
$$J_{diff} = -\varphi D_s(\partial C/\partial z). \tag{2}$$

Figure 7. Comparison of NO_3^- and denitrification flux estimates as a function of plug thickness, using either linear gradient approximations (solid symbols) to measured concentrations between sample intervals or a diffusion reaction model (open symbols) having a zone of constant nitrification overlying a denitrification zone (Eq. 3, text, Figure 8). (A) Flux of NO_3^- into overlying water as function of plug thickness. (B) Flux of NO_3^- into underlying sediment (denitrification). (C) Total sedimentary nitrification flux (total NO_3^- production). (D) Ratio of denitrification to total nitrification. In all cases optimal (maximum) rates and maximum relative denitrification occurs in the 5 mm plug.

Flux estimates were obtained by assuming linear concentration gradients between adjacent sampling intervals and by assigning measured concentrations to the mid-point of sample intervals or to the sediment surface in the case of overlying water (assuming no significant diffusive boundary layers). The whole sediment diffusion coefficient for NO_3^- was estimated from the free solution value, D_o, corrected for temperature ($T = 22°C$), salinity, and tortuosity using the Archie-type relation: $D_s \sim \varphi^2 D_o$ (Li and Gregory, 1974; Ullman and Aller, 1982; Boudreau, 1997). Total nitrification fluxes were calculated from the sum of the upward and downward diffusive fluxes supported by sedimentary NO_3^- gradients. Denitrification was defined from this standpoint as the total flux of NO_3^- into sediment. The 5 mm plug had the highest net nitrification fluxes, the highest denitrification flux, and the highest ratio of denitrification to total nitrification (Fig. 7). The thin plug (2 mm) supported net NO_3^- fluxes comparable to the thickest sediment layers despite substantially lower volume of reacting material. Increased total net DIN remineralization as sediment thickness decreases is consistent with the DIN mass balance calculations made previously.

Table 2. Model flux values: linear gradient and constant nitrification rate estimates*.

Plug thickness, L_2 (mm)	Nitrification zone thickness, L_1 (mm)	Denitrification rate constant, k_d (d^{-1})	ΣNO_3^- flux** (μmol cm^{-2} d^{-1})	Denitrification flux (μmol cm^{-2} d^{-1})
2 (gradient)			0.47	0
2	2	0	0.53	0
5 (gradient)			1.14	0.28
5	1	60.4	1.84	0.45
10 (gradient)			0.58	0.077
10	2	10.1	0.75	0.17
20 (gradient)			0.68	0.17
20	1	1.7	0.50	0.052

*Model equation 3.
**Sum of upward and downward flux of NO_3^- from production zone.

g. Diffusion reaction models–average reaction rates

Estimates of the average reaction rates over specific intervals of plug sediments were also obtained from a simple two zone transport-reaction model evaluated at steady state (Vanderborght and Billen, 1975; Billen, 1982; Jahnke *et al.,* 1982). The small thicknesses of the plugs, the N-compound concentration patterns in the overlying water, and sampling time should have ensured that distributions in the plugs were at a pseudo-steady state (see subsequent section). In each plug set, it was assumed that an upper zone of net nitrification overlaid a zone of net denitrification. Nitrification rate was approximated as constant over the oxygenated interval depth L_1, and denitrification was taken as a first order reaction with respect to NO_3^- concentration. The model equations and boundary conditions are:

$$\text{Zone 1 (nitrification) } (0 \leq z \leq L_1): D_s(\partial^2 C_1/\partial z^2) + R_{NO} = 0 \qquad (3a)$$

$$\text{Zone 2 (denitrification) } (L_1 \leq z \leq L): D_s(\partial^2 C_2/\partial z^2) - k_{dN}C_2 = 0 \qquad (3b)$$

$$\text{Boundary conditions: } z = 0, \ C_1 = C_T; \ z = L, \ \partial C_2/\partial z = 0 \qquad (3c)$$

$$z = L_1, \ C_1 = C_2, \ \partial C_1/\partial z = \partial C_2/\partial z$$

The value of L_1 for each plug group was set equal to the base of the sample interval in which the maximum NO_3^- concentration was measured. We found that if the entire measured penetration depth of O_2 was used (see subsequent discussion), it was not possible to obtain even moderately accurate fits to the NO_3^- distributions if a constant nitrification rate were also used. The analytical solution $C(z)$ to Eqs. 3a–c was integrated (averaged) over the finite intervals 0–1 mm, 1–2 mm, and $2 - L$ corresponding to the sampling depths. Optimal values of R_{NO} (zeroth order nitrification rate) and k_{dN} (denitrification rate constant) were then estimated from simultaneous best fits of the integral solutions to the average NO_3^- values using the Levenberg-Marquardt method (Table 2; Fig. 8). The nitrification and denitrification fluxes so obtained were consistently higher than those
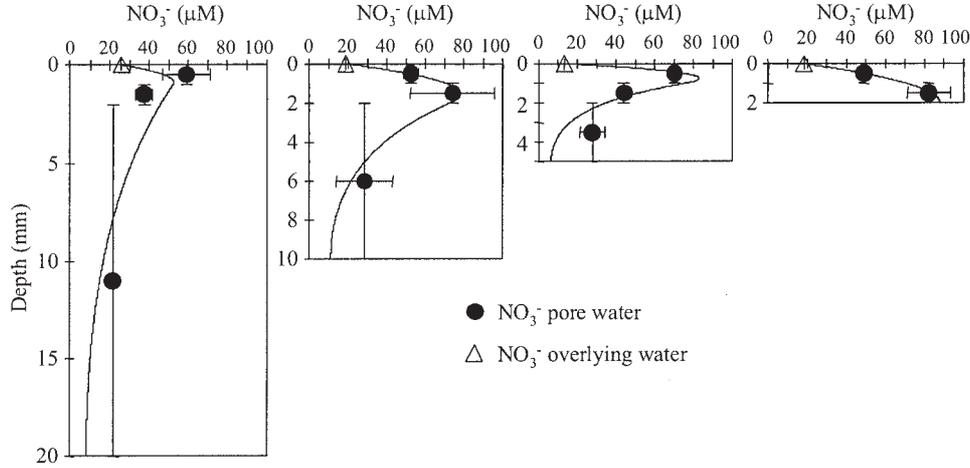
Figure 8. NO_3^- pore water profiles in plugs (from Figure 5; mean $\pm$ SD), overlying water is plotted as an open triangle. The continuous curves represent diffusion reaction model fits using equation 3 (surface zone of constant nitrification rate over interval L_1, first order denitrification in underlying zone).

derived from the simple linear gradient approximations using equation (2), but clearly showed the same relative reaction rate patterns (Fig. 7), that is, maximum rates and optimal (e.g., maximum ratio of denitrification/nitrification) coupling between oxic and anoxic zones in the 5 mm plugs. The whole sediment NO_3^- diffusion coefficient in each case was estimated as described previously.

h. Coupled models and kinetics of nitrification/denitrification

The distribution patterns of O_2, NO_3^-, and NH_4^+ were further examined using more sophisticated coupled transient and steady state diffusion–reaction models in order to evaluate the assumptions of steady state, different possible concentration dependent forms for nitrification reaction kinetics, and most importantly in the present cases, the scale–dependent reaction balances during the experiment. For example, one characteristic of the NO_3^- (and NO_2^-) profiles that cannot be reproduced well by a constant, average nitrification rate as used above, is the near surface (0–1 mm) maximum found in the 5 and 20 mm plugs (Figs. 5, 6). Three different kinetic functions for nitrification, R_{NO3}, were considered here:

$$R_{NO3} = v_{NO3}(O_2)(NH_4^+)/[((O_2) + K_{O2,NO3})((NH_4^+) + K_{NH4,NO3})] \tag{4a}$$

$$R_{NO3} = k_{NO3}(O_2)(NH_4^+) \tag{4b}$$

$$R_{NO3} = k_{NO3}^*(O_2)^2(NH_4^+) \tag{4c}$$

The hyperbolic kinetic Eq. (4a) is based on the experimentally measured responses of pure cultures of ammonia oxidizing and nitrifying bacteria to varying concentrations of O_2 and NH_4^+ (Brion and Billen, 1998) (NH_4^+ represents total dissolved ammonia species in all

cases). The constants v_{NO3}, $K_{O2,NO3}$, and $K_{NH4,NO3}$ correspond to maximum reaction rate and half saturation constants for O_2 and NH_4^+ respectively. Maximum reaction, v_{NO3}, depends directly on local biomass (Brion and Billen, 1998). The second order kinetic form with fixed rate constant k_{NO3}, Eq. (4b), was successfully employed by Van Cappellen and Wang (1996) as a likely approximation for overall nitrification kinetics in surface sediments. Eq. (4c) was also utilized here as a possible phenomenological alternative consistent with overall reaction stoichiometry but without a previous observational basis.

The overall model formulation follows the hyperbolic oxidant consumption and serial inhibition approach of Rabouille and Gaillard (1991) and Van Cappellen *et al.* (1993), so that for the dissolved species set (i), $(i = O_2, NO_3^-, NH_4^+)$:

$$(1 + K_i)\partial(i)/\partial t = D_{s,i}(\partial^2(i)/\partial z^2) + \Sigma R_i \tag{5}$$

with:

$$\Sigma R_{O2} = -\sigma_{O2}v_C(O_2)/(K_{C,O2} + (O_2)) - R_{NO3}$$
$$\Sigma R_{NO3} = R_{NO3} - \sigma_{NO}v_C(NO_3)(\text{Inhibit}_{O2,NO3})/(K_{C,NO3} + (NO_3))$$
$$\Sigma R_{NH4} = \sigma_{NH}v_C - R_{NO3}$$
$$v_C = \text{maximum organic C oxidation rate}$$
$$\sigma_{O2}, \sigma_{NO}, \sigma_{NH} = \text{stoichiometric reaction ratios } O_2/C, NO_3/C, \text{ and } NH_4^+/C$$
$$\text{Inhibit}_{O2,NO3} = K_{I,O2,NO3}/(K_{I,O2,NO3} + (O_2))$$
$$K_{I,O2-NO3} = \text{inhibition constant for } O_2 \text{ on denitrification}$$
$$K_i = \text{reversible adsorption coefficient } (=0 \text{ for } O_2, NO_3^-)$$

Qualitatively, this set of coupled equations accounts for diffusive transport, the uptake of O_2 by aerobic respiration and nitrification, the uptake and production of NO_3^- by denitrification and nitrification, and the production and consumption of NH_4^+ during ammonification and nitrification. The inhibition of denitrification by aerobic activity was incorporated in the inhibition function, Inhibit_{O2-NO3}, with $K_{I,O2-NO3} = 1\,\mu M$ as an approximation (Humphrey, 1972; Boudreau, 1997). The equation set was evaluated using a fully explicit finite difference routine for the initial and boundary conditions:

$$t = 0, \ 0 \leq z \leq L, \ (i) = (i)_0; \ t > 0, \ z = 0, \ (i) = (i)_T$$

$$z = L, \ \partial(i)/\partial z = 0$$

Numerical solutions were stable and mass balances maintained over the range of evaluation. Whole sediment diffusion coefficients were estimated in each case from the free solution values at 22°C assuming the Archie-type relation given previously.

Examples of steady state distributions of O_2, NO_3, and NH_4^+ for a 5 mm plug are shown in Figure 9. In all cases, model examples assume: $v_c = 3.5$ mM d^{-1}; $\sigma_{O2}, \sigma_{NO}, \sigma_{NH} = 1$, 0.8, and 0.2; $K_{C,O2} = 10\,\mu M$; $K_{C,NO3} = 10\,\mu M$; and a reversible adsorption constant $K_{NH4} = 0.91$ (Green *et al.,* 1998). Overlying water concentrations were fixed at 240, 13.5, and 0 μM for O_2, NO_3, and NH_4^+ respectively. Model I assumes nitrification kinetics (R_{NO3}, Eq. 4a) with $v_{NO3} = 50$ mM d^{-1}; $K_{O2,NO3} = 20\,\mu M$; $K_{NH4,NO3} = 100\,\mu M$ (half
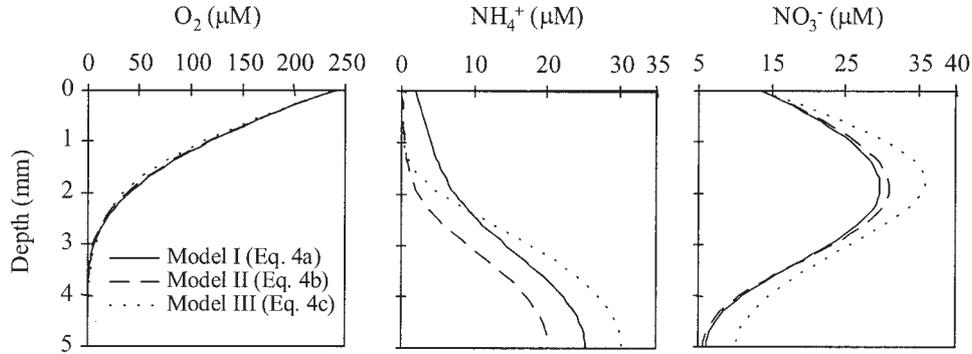
Figure 9. Example steady state model profiles of O_2, NH_4^+, and NO_3^- for the 3 nitrification kinetic functions outlined in text. The subsurface NO_3^- maximum cannot occur in the surface $0-1$ mm interval without major changes in kinetic parameters, additional reactions not accounted for, or relative rates of remineralization (e.g. increased N/C ratio).

saturation constants after Brion and Billen, 1998). Model II assumes overall second order kinetics (R_{NO3}, Eq. 4b) with $k_{NO3} = 30\ \mu M^{-1}\ d^{-1}$. Model III assumes nitrification kinetics second order in O_2 and first order in NH_4^+ (R_{NO3}, Eq. 4c), with $k_{NO3}^* = 0.5\ \mu M^{-2}\ d^{-1}$. These values were chosen to produce simultaneous approximations to the profiles primarily for purposes of illustration of basic principles and relative behavior rather than for optimal fits to individual data sets.

Steady state (pseudo) was achieved in ~ 0.2 ($L = 2$ mm) to ~ 4 days ($L = 20$ mm) for a wide range of potential reaction rates that were broadly constrained by observed concentration distributions. The use of a constant overlying water boundary condition in model calculations is therefore a good approximation given the slow rate of change in water properties over the last several days of the experiment (Fig. 3). A primary conclusion of these calculations is that it was not possible to simulate NO_3^- maxima in the upper $0-1$ mm of plugs with any combination of reaction rates using forms of Eq. (4) that were simultaneously consistent with O_2, NO_3^-, and NH_4^+ distributions (and HCO_3^- distributions, Aller *et al.,* in preparation) and with the magnitude of observed fluxes. The NO_3^- distributions require a far higher nitrification rate at the sediment–water interface and also require maximum nitrification to occur at a much higher average O_2 than can be accounted for by the assumed kinetic functions. These results are consistent with the need to restrict nitrification in the model Eq. (3) to intervals less than the penetration depth of O_2.

The model calculations (Eq. 4) using a fixed overall ammonification rate ($\sigma_{NH}v_C$) in all cases demonstrate that the relative rates of nitrification/ammonium production, denitrification/nitrification, denitrification/ammonium production, and nitrification/total oxygen flux should vary regularly with plug thickness at steady state regardless of the assumed kinetics of nitrification (Fig. 10). Because the overall ammonification rate is constant (volumetric), the steady flux of NH_4^+ into the oxic zone increases linearly with plug thickness. The proportion of the oxygen flux utilized by nitrification increases, and the oxygen penetration
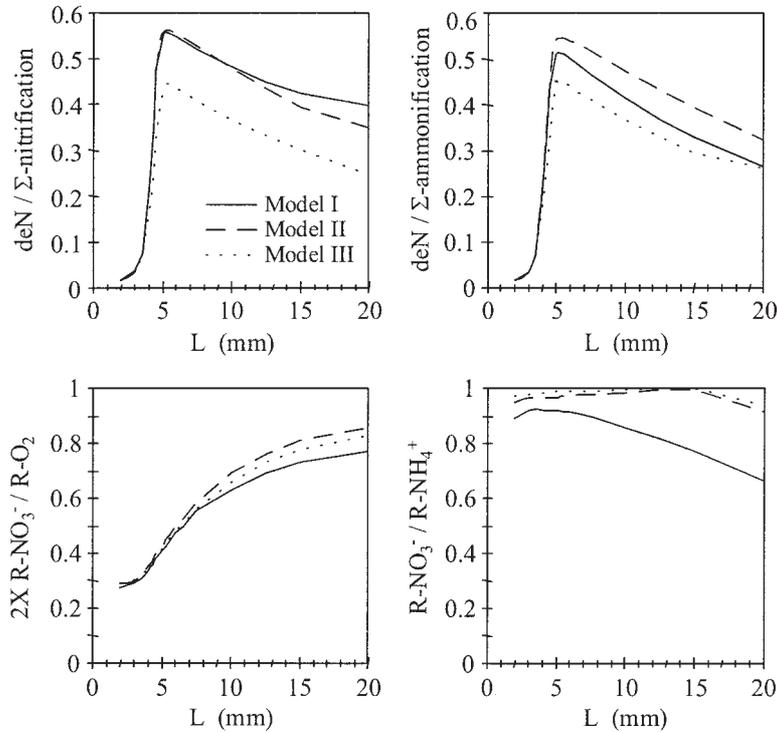
Figure 10. Model calculations demonstrating steady state reaction balances as a function of both diffusion scale and three different nitrification kinetic functions (Eqs. 4a.b.c) in planar geometries comparable to the experimental sediment plugs. The maximum C_{org} remineralization rate is fixed at 3.5 mM d^{-1} and the N/C ammonification ratio at 0.2 (see text). Model I assumes hyperbolic nitrification kinetics (Eq. 4a), Model II first order kinetics in both O_2 and NH_4^+, and Model III second order in O_2, first order in NH_4^+ (see text). Maximum denitrification relative to nitrification and ammonification occurs between 5–6 mm scaling. Note the proportion of the O_2 flux utilized for other than C_{org} oxidation increases steadily with sediment thickness and becomes progressively dominated by reoxidation of anaerobic metabolites.

depth decreases, as the flux into the oxic zone of reduced metabolites (solely NH_4^+ in these model considerations) from the anoxic zone, increases with sediment thickness (Figs. 10, 11). Total nitrification fluxes increase directly with plug thickness (results not shown), eventually reaching a maximum determined by the maximum supply of O_2, the specific nitrification kinetics, and competition with additional reductants entering the oxic zone. The planar models predict that about ~30–50% of the remineralized N should be denitrified, depending on the exact reaction kinetics and relative scaling of the redox zones. Optimal couplings between nitrification, denitrification, and ammonification (highest denitrification/nitrification; highest denitrification/ammonification) are achieved at sediment scales between 5–10 mm for the general remineralization rates in the experimental sediment.
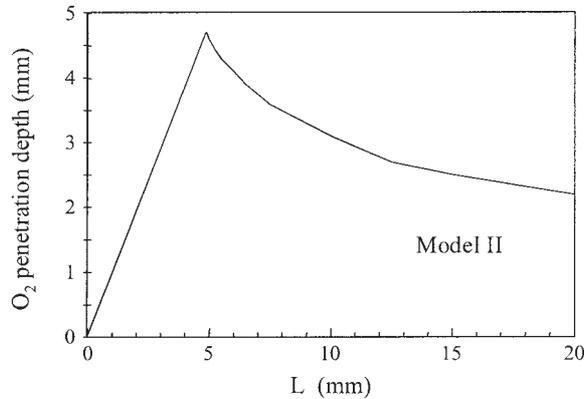
Figure 11. Example O_2 penetration depth ($\geq 0.1\ \mu M$ concentration depth) predicted by Model 2 nitrification kinetics (Eq. 4b, $1^\circ\ O_2$, $1^\circ\ NH_4^+$) as a function of sediment thickness (Model values as in Fig. 8, 9 and text). If higher levels of O_2 concentration are used to define penetration depth (e.g. $\geq 10\ \mu M$), similar relative patterns are obtained but the linear portion is contracted and maximum penetration depth occurs at a smaller L.

4. Discussion

Our experimental and model results demonstrate that small changes in the thicknesses of adjacent oxic–anoxic zones result in significant differences in both the absolute and relative rates of nitrification and denitrification in sediments. The scale-dependent changes in redox reactions in our experimental sediment plugs presumably mimic to various extents those attained in portions of bioturbated deposits as any two oxygenated burrow centers move closer (thin plugs) or farther apart (thick plugs) (Fig. 1). It is, therefore, clear that nitrification–denitrification interactions in the bioturbated zone are a function of burrow spacing, size (radii), and nearest neighbor diffusive interactions in addition to local sediment properties determined by species-specific activities (Fig. 4).

a. Nitrification

The primary source of NO_3^- for sedimentary denitrification is normally NO_3^- formed within the oxic sediment zone adjacent to the oxygenated water boundary (Billen, 1982). The rate of NO_3^- formation depends on the diffusive supply of O_2 and NH_4^+, nitrification kinetics (including specific properties of bacterial populations), and competition between various reductants (e.g. C_{org}, DOC, NH_4^+, H_2S, Fe^{++}, Mn^{++}) for O_2. The diffusive flux of NH_4^+ increases linearly with plug thickness whereas the O_2 flux reaches a maximum value limited by overlying water concentration and diffusive transport (Jørgensen, 2001). Nitrification rates should therefore increase with plug thickness (burrow spacing) and likely plateau (saturate) or begin to decrease, depending on the exact competitive relations of NH_4^+ with additional reductants supplied to the oxic zone. Overall, nitrification should consume a progressively greater proportion of the O_2 flux as anoxic zone thickness increases (Fig. 10).

The experimental results show a distinct maximum in nitrification rates in the 5 mm plugs compared to thinner (2 mm) or thicker plugs (10, 20 mm) (Fig. 7). Whereas the increase of nitrification rate in the 5 mm plug relative to the thinner 2 mm plug is expected from the increased NH_4^+ flux from the anoxic zone, the large decrease of nitrification rate in plugs with larger ratios of anoxic/oxic zone thicknesses (i.e. the 10 and 20 mm plugs) must reflect: (1) higher fluxes of NH_4^+ into the oxic zone of the 5 mm plug relative to thicker plugs; and/or, (2) increased fluxes of competing reductants into the oxic zone of the thicker plugs.

There is strong previous experimental evidence that increased transport efficiency of solutes and decreased metabolite build-up affect net remineralization rates in sediments. In completely anoxic sediment, net remineralization rate, as measured by NH_4^+ release, increases as diffusive scale (plug thickness) and metabolite buildup decrease (Aller and Aller, 1998). Our present results are consistent with those findings in that the maximum in nitrification rate in the 5 mm plugs suggests an enhanced net flux of NH_4^+ into the oxic zone relative to thicker plugs despite the greater potential source in the latter. As noted earlier (Eq. 1), the release of inorganic N from plugs into the overlying water reservoirs also indicate increased net remineralization of N as plug thickness decreased. Thus, at least a portion of the maximum nitrification rate observed at the intermediate plug scale length (5 mm) may reflect an optimal balance between diffusive supply of O_2 and an enhancement of net ammonification rate in the anoxic zone as overall diffusive scale decreases.

Regardless of whether the net remineralization rate (volumetric) is a function of transport scale, the steady flux of reduced solutes into the oxic zone must eventually increase as total anoxic zone thickness increases (integration of the volumetric rate with depth). As a result, the oxic zone becomes thinner as overall plug thickness increases, and the region within which aerobic nitrification can occur contracts (Figs. 4, 11). This contraction of the oxic zone must accentuate competition between possible reductants for O_2 and may further contribute to the decrease in net nitrification as the ratio of anoxic/oxic zone volumes increases.

The measured NO_3^- distributions are consistent with the concept that competition between reductants can be an important influence on sedimentary nitrification. We observed the maximum net nitrification in regions of relatively high O_2 near the sediment-water interface (Figs. 4, 5) and not at the redoxcline where O_2 is low and NH_4^+ high. These observations have been confirmed by additional, very detailed transient state experiments similar in design to the present experiments (Eriksson and Aller, 2001). The shift of the highest NO_3^- concentrations toward the sediment-water interface (first sample interval) could not be reproduced by any of the nitrification or remineralization model kinetic functions (Eqs. 3, 4) used here, when distributions were also constrained by the O_2 penetration depth and NH_4^+ profiles (i.e. remineralization rate). Model fits using a simple constant nitrification rate (Eq. 3; Fig. 8) are not accurate unless O_2 penetration depths (i.e. nitrification zone) are restricted to intervals $<0.5 \times$ the actual value, for example 1 mm rather than 3 mm (Fig. 8; plug 5 mm). These findings suggest that, for example, the O_2 half saturation constant (Eq. 4a) derived from laboratory studies of pure cultures (Brion and

Billen, 1998) is actually far higher (e.g. >100 μM compared to $\sim 10–20$ μM) in natural sediments with mixed populations and competing reactions. It was for this reason that a second order kinetic dependence on O_2 concentration (Eq. 4c), which shifts maximum nitrification rates toward higher O_2, was also utilized as a possible kinetic form in our calculations. The functional ecological effect of a shift of nitrification to higher O_2 is to decrease reaction competition with other reductants produced during anaerobic metabolism.

Our data and models show that for a variety of reasons, sedimentary nitrification is a strong function of both the absolute and relative scaling of adjacent oxic and anoxic zones. A maximum rate of nitrification is achieved under particular spatial scales that allow for optimal balances between O_2 flux, NH_4^+ production rates in adjacent oxic/anoxic zones, and the fluxes of competitive metabolites into the oxic zone. These optimal nitrification conditions were found in the present case for diffusive transport scales typically observed in the bioirrigated zone, equivalent to ~ 1 cm between oxygenated boundaries (or ~ 5 mm half-distance between burrows).

b. Coupled nitrification–denitrification

As in the case of nitrification, a number of factors determine the rate of denitrification and the coupling of reactions between oxic and anoxic zones. Coupling between zones consists of the flux of NH_4^+ and reduced metabolites from the anoxic into the oxic zone, and the return flux of NO_3^- from the oxic into the denitrification zone. The distance between the oxygenated overlying water boundary (irrigated burrow center) and the reflective boundary at the base of the plugs (approximately midway between irrigated burrow centers) controls the overall transport scale and the relative abundances of oxidants (O_2, NO_3^-) and reductants (NH_4^+). Given the remineralization rates in the experimental sediment, the sediment became fully oxygenated and denitrification was hindered by O_2 for sediment thicknesses <5 mm (e.g., Payne, 1976; Kapralek *et al.*, 1982) (Figs. 4, 6, 11). As sediment thickness increased to ~ 5 mm, nitrification increased to a maximum for the reasons discussed previously. Denitrification varied in direct proportion to nitrification, also reaching an optimum (maximum) rate in the 5 mm thick plug (Fig. 6).

Regardless of whether net remineralization rates (NH_4^+ production) increase with a decrease in overall diffusive transport scale, changes in the relative rates and coupling of reactions between zones must occur. Model calculations demonstrate that the proportion of denitrification/nitrification and denitrification/ammonification in plugs first reach maxima and then decrease as anoxic zone thicknesses increase (Fig. 10). Nitrification consumes a progressively larger proportion of the O_2 flux as overall sediment thickness increases, but a larger proportion of total NH_4^+ production (flux) escapes as nitrification kinetics in the oxic zone become saturated (Fig. 10). The decrease in denitrification with increasing plug thickness >5 mm also reflects the fact that a greater proportion of the NO_3^- formed is lost into the overlying water as the oxic zone contracts and the NO_3^- maximum moves closer to the sediment-water interface. For the present illustrative calculations, we assumed that reaction kinetic parameters such as reaction rate constants (e.g. k_{NO3}, Eq. 4b) do not

change with overall scale (i.e. are not a function of metabolite inhibition of net remineralization, competition between reductants for O_2, etc.). The dependence of reaction balances on diffusion scale are even more accentuated if net remineralization rate (volumetric) varies inversely with thickness and competition between reductants for O_2 are considered.

Therefore at a given remineralization (ammonification) rate there are particular scales of oxic and anoxic zones that produce maximum rates of reactions and maximum efficiency of reaction coupling between zones (e.g., maximum denitrification/nitrification, maximum denitrification/ammonification). In the case of denitrification, for example, the penetration of NO_3^- into underlying sediment becomes a progressively smaller proportion of the total anoxic region as plug thickness increases. The simultaneous contraction of the nitrification zone with plug thickness accentuates this proportional decrease. If denitrification is assumed to be a first order reaction in NO_3^-, (Eq. 3b), the lengthscale of NO_3^- penetration into the anoxic zone is $\sim \sqrt{D_s/k_{dN}}$. Thus, increasing the thickness of the anoxic zone beyond that scale does not optimally couple ammonification and nitrification to increased denitrification.

c. Extrapolation to the bioirrigated zone and natural conditions

For the experimental sediment used here, maximum rates and optimal coupling between aerobic and anaerobic reactions occurred in planar geometries for sediment thicknesses of ~ 5 mm. This overall scale would correspond roughly to evenly spaced burrow structure abundances of ~ 3000–$11,000$ m^{-2}, depending on the radius of the oxygenated burrows involved (e.g., $r = 0.05$–0.5 cm). For smaller and larger thicknesses (diffusive lengthscales), a combination of factors decreased the overall efficiency of coupling between zones. The exact scaling of interactions between reactions in adjacent oxic and anoxic zones is affected by radial geometries, such as typically characterize the regions around irrigated burrows, and can only be approximately simulated by planar geometries (Aller, 1988, 2001; Fig. 1). In addition, the effective scaling between oxygenated burrow microenvironments is also determined by various aspects of burrowing behavior, including burrow generation rates, burrow longevity, and irrigation frequency (burrow lumen boundary conditions). For example, active burrowers or tube-builders can produce enhanced effects at lower population densities than sedentary species (Woodin and Marinelli, 1991). Even for sedentary species, burrow size, orientation, and spacing are commonly highly variable locally and change with time. Statistical distributions of community burrow patterns in space and time are therefore most properly considered in quantitative models of average transport-reaction geometries (Gilbert *et al.,* 1995; Furukowa *et al.,* 2001; Koretsky *et al.,* 2002).

There are also other, theoretically possible, sedimentary nitrification and NO_3^- reduction reactions which may be affected by biogenic transport processes and which were not included in our considerations. For example, anaerobic nitrification can apparently occur through a Mn-oxide reduction pathway in which the flux of Mn-oxide is largely determined by bioturbation (Luther *et al.,* 1997; Hulth *et al.,* 1999; Anschutz *et al.,* 2000). The NO_3^- profiles in basal regions of plugs and their departure from the simplest model predictions in

the present experiments hint at the occurrence of such anaerobic nitrification reactions (Fig. 7). The reduction of NO_3^- by alternative reductants such as NH_4^+ may also occur and further complicate reaction kinetics and zonal coupling (Thamdrup and Dalsgaard, 2000).

The quantitative results derived from this study should not be directly extrapolated without additional modifications to natural bioturbated deposits. For example, species-specific characteristics such as mucus secretion, particle selection, bioirrigation activity patterns, and additional factors such as C_{org} flux to the sediment surface, are important controls on sedimentary redox reactions. Our experiments did not incorporate interstitial advection of pore water that can occur around biogenic structures in highly permeable sands (Huettel and Webster, 2001). The possible roles of meiofauna in altering reaction rates and local transport were also not explicitly examined (e.g., Reichelt *et al.,* 1991). Our experiments and models clearly demonstrate; however, that whatever the burrowing organisms involved, the balance between stimulation/inhibition of denitrification and N remineralization is highly dependent on burrow or irrigated microenvironment distribution and associated diffusion–reaction structure. A greater effort to statistically document geometric relations (scaling distributions) between oxic–anoxic zones within bioturbated deposits is clearly required for quantitative interpretation and predictive modeling of sedimentary N cycling.

5. Conclusions

Irrigated burrow structures produce complex patterns of oxic–anoxic microenviron-ments in the bioturbated zone.

A major property determining the absolute and relative rates of sedimentary redox reactions such as nitrification–denitrification is the characteristic transport scale set by burrow lumen size and the spacing of oxygenated burrow centers.

The dependence of coupled redox reactions such as nitrification–denitrification on oxic–anoxic zonal scaling around and between burrows can be simulated in part by plugs of variable sediment thickness exposed on one surface to oxygenated water. For a given remineralization rate (reactive C_{org}), an optimal scaling exists which simultaneously maximizes nitrification, denitrification, the ratio of denitrification/nitrification, and the ratio of denitrification/ammonification.

Common size and abundance ranges of infaunal communities can apparently readily achieve optimal reaction scalings for nitrification–denitrification.

The *in-situ* kinetics of nitrification in the oxic zone of organic rich sediments are not well constrained by presently accepted relationships, implying that natural populations of nitrifiers must be utilized in future kinetic studies of the dependence of aerobic nitrification on O_2, NH_4^+, and the simultaneous presence of multiple anaerobic metabolites.

Redox reaction coupling during the sedimentary cycling of N in the bioirrigated zone has the potential for far greater complexity than has been commonly appreciated.

REFERENCES

Aller, R. C. 1984. The importance of relict burrow structures and burrow irrigation in controlling sedimentary solute distributions. Geochim. Cosmochim. Acta, *48,* 1929–1934.

——1988. Benthic fauna and biogeochemical processes in marine sediments: the role of burrow structures, *in* Nitrogen Cycling in Coastal Environments, T. H. Blackburn and J. Sørensen, eds., John Wiley and Sons, 301–338.

——2001. Transport and reactions in the bioirrigated zone, *in* The Benthic Boundary Layer: Transport Processes and Biogeochemistry, B. Boudreau and B. B. Jørgensen, eds., Oxford Press, 269–301.

Aller, R. C. and J. Y. Aller. 1998. The effect of biogenic irrigation intensity and solute exchange on diagenetic reaction rates in marine sediments. J. Mar. Res., *56,* 905–936.

Aller, J. Y., R. C. Aller and M. A. Green. 2002. Benthic faunal assemblages and carbon supply along the continental shelf/shelf break-slope off Cape Hatteras, North Carolina. Deep Sea Res. II, *49,* 4599–4625.

Aller, R. C. and J. E. Mackin. 1989. Open-incubation, diffusion methods for measuring solute reactions rates in sediments. J. Mar. Res., *47,* 411–440.

Aller, R. C., J. Y. Yingst and W. J. Ullman. 1983. Comparative biogeochemistry of water in interdidal *Onuphis* (Polychaeta) and *Upogebia* (Crustacea) burrows: temporal patterns and causes. J. Mar. Res., *41,* 571–604.

Anschutz, P., B. Sundby, L. Lefrançois, G. W. Luther III and A. Mucci. 2000. Interactions between metal oxides and species of nitrogen and iodine in bioturbated marine sediments. Geochim. Cosmochim. Acta, *64,* 2751–2763.

Balderston, W. L., B. Sherr and W. J. Payne. 1976. Blockage by acetylene of nitrous oxide production in *Pseudomonas perfectomarinus.* Appl. Environ. Microbiol., *81,* 504–508.

Berelson, W. M., D. Heggie, A. Longmore, T. Kilgore, G. Nicholson and G. Skyring. 1998. Benthic nutrient recycling in Port Phillip Bay, Australia Estuar. Coast. Shelf Sci., *46,* 917–934.

Berner, R. A. 1980. Early Diagenesis: A Theoretical Approach, Princeton University Press, 241 pp.

Billen, G. 1982. An idealized model of nitrogen recycling in marine sediments. Am. J. Sci., *282,* 512–541.

Boudreau, B. P. 1996. The diffusive tortuosity and porosity of fine-grained sediments. Geochim. Cosmochim. Acta, *60,* 3139–3142.

——1997. Diagenetic Models and Their Implementation, Springer-Verlag, 414 pp.

Boudreau, B. P. and R. L. Marinelli. 1994. A modeling study of discontinuous biological irrigation. J. Mar. Res., *52,* 947–968.

Brion, N. and G. Billen. 1998. Une réévaluation de la methode d'incorporation de $H^{14}CO_3^-$ pour mesurer la nitrification autotrophe et son application pour estimer des biomasses de bacteries nitrifantes. Rev. Sci. Eau, *11,* 283–302.

Eriksson, S. P. and R. C. Aller. 2001. Transient to steady biogeochemical succession in organic-rich marine sediment. ALSO Spring Meeting, Albuquerque, New Mexico.

Firestone, M. K., R. B. Firestone and J. M. Tiedje. 1980. Nitrous oxide from soil denitrification: factors controlling its biological production. Science, *208,* 749–751.

Furukawa, Y., S. J. Bentley and D. L. Lavoie. 2001. Bioirrigation modeling in experimental benthic mesocosms. J. Mar. Res., *59,* 417–452.

Gérino, M., R. C. Aller, C. Lee, J. K. Cochran, J. Y. Aller, M. A. Green and D. Hirschberg. 1998.

Comparison of different tracers and methods used to quantify bioturbation during a spring bloom: 234-thorium, luminophores and Chlorophyll *a*. Estuar. Coast. Shelf Sci., *46,* 531–547.

Gilbert, F., P. Bonin and G. Stora. 1995. Effect of bioturbation on denitrification in a marine sediment from the West Mediterranean littoral. Hydrobiologia, *304,* 49–58.

Gilbert, F., G. Stora and P. Bonin. 1998. Influence of bioturbation on denitrification activity in Mediterranean coastal sediments: an in situ experimental approach. Mar. Ecol. Progr. Ser., *163,* 99–107.

Green, M., R. C. Aller and J. Y. Aller. 1998. The influence of carbonate dissolution on the survival of shell-bearing meiobenthos in nearshore sediments. Limnol. Oceanogr., *43,* 18–28.

Hall, P. O. J. and R. C. Aller. 1992. Rapid, small volume, flow injection analysis for ΣCO_2 and NH_4^+ in marine and freshwaters. Limnol. Oceanogr., *37,* 1113–1119.

Henriksen, K. and M. W. Kemp. 1988. Nitrification in estuarine and coastal marine sediments: methods, patterns and regulating factors, *in* Nitrogen Cycling in Coastal Environments, T. H. Blackburn and J. Sørensen, eds., John Wiley and Sons, 207–249.

Huettel, M. and I. T. Webster. 2001. Porewater flow in permeable sediments, *in* The Benthic Boundary Layer: Transport Processes and Biogeochemistry, B. Boudreau and B. B. Jørgensen, eds., Oxford Press, 144–179.

Hulth, S., R. C. Aller and F. Gilbert. 1999. Coupled anoxic nitrification/manganese reduction in marine sediments. Geochim. Cosmochim. Acta, *63,* 49–66.

Humphrey, A. E. 1972. The kinetics of biosystems: a review, *in* Chemical Reaction Engineering, R. F. Gould, ed., ACS Adv. Chemistry Ser., *109,* 630–650.

Jahnke, R. A., S. R. Emerson and J. W. Murray. 1982. A model of oxygen reduction, denitrification, and organic matter mineralization in marine sediments. Limnol. Oceanogr., *27,* 610–623.

Jørgensen, B. B. 2001. Life in the diffusive boundary layer, *in* The Benthic Boundary Layer: Transport Processes and Biogeochemistry, B. Boudreau and B. B. Jørgensen, eds., Oxford Press, 348–373.

Kapralek, F., E. Jechova and M. Otavova. 1982. Two sites of oxygen control in induced synthesis of respiratory nitrate reductase by *Escherichia coli*. J. Bact., *149,* 1142–1145.

Knowles, R. 1982. Denitrification. Microbiol. Rev., *46,* 43–70.

Koretsky, C. M., C. Meile and P. Van Cappellen. 2002. Quantifying bioirrigation using ecological parameters: a stochastic approach. Geochemical Transactions, *3,* 17–30.

Kristensen, E. 1988. Benthic fauna and biogeochemical processes in marine sediments: microbial activities and fluxes, *in* Nitrogen Cycling in Coastal Environments, T. H. Blackburn and J. Sørensen, eds., John Wiley and Sons, 275–299.

Kristensen, E. and T. H. Blackburn. 1987. The fate of organic carbon and nitrogen in experimental marine sediment systems: Influence of bioturbation and anoxia. J. Mar. Res., *45,* 231–257.

Kristensen, E., M. H. Jensen and R. C. Aller. 1991. Direct measurement of dissolved inorganic nitrogen exchange and denitrification in individual polychaete (*Nereis virens*) burrows. J. Mar. Res., *49,* 355–377.

Kristensen, E., M. H. Jensen and T. K. Andersen. 1985. The impact of polychaete (*Nereis virens* Sars) burrows on nitrification and nitrate reduction in estuarine sediments. J. Exp. Mar. Biol. Ecol., *85,* 75–91.

Li, Y. H. and S. Gregory. 1974. Diffusion of ions in seawater and deep-sea sediments. Geochim. Cosmochim. Acta, *38,* 703–714.

Luther, G. W., III, B. Sundby, B. L. Lewis, P. J. Brendel and N. Silverberg. 1997. Interactions of manganese with the nitrogen cycle: alternative pathways to dinitrogen. Geochim. Cosmochim. Acta, *61,* 4043–4052.

Mayer, M. S., L. S. Schaffner and W. M. Kemp. 1995. Nitrification potentials of benthic macrofaunal tubes and burrow walls: effects of sediment NH_4^+ and animal irrigation behavior. Mar. Ecol. Progr. Ser., *121,* 157–169.

Payne, W. J. 1976. Reduction of nitrogenous oxides by microorganisms. Bact. Rev., *37,* 409–452.

Pelegri, S. P., L. P. Nielsen and T. H. Blackburn. 1994. Denitrification in estuarine sediment stimulated by the irrigation activity of the amphipod *Corophium volutator.* Mar. Ecol. Progr. Ser., *105,* 285–290.

Rabouille, C. and J.-F. Gaillard. 1991. A coupled model representing the deep-sea organic carbon and oxygen consumption in surficial sediments. J. Geophys. Res., *96,* 2761–2776.

Reichelt, A. C. 1991. Environmental effects of meiofaunal burrowing, *in* The Environmental Impact of Burrowing Animals and Animal Burrows, P. S. Meadows and A. Meadows, eds., A. Zool. Soc. London Symposia, *63,* 33–52.

Revsbech, N. P., J. Sørensen and T. H. Blackburn. 1980. Distribution of oxygen in marine sediments measured with microelectrodes. Limnol. Oceanogr., *25,* 403–411.

Ronan, T. E., Jr. 1978. Food-resources and the influence of spatial pattern on feeding in the phoronid *Phoronopsis viridis.* Biol. Bull., *154,* 472–484.

Rysgaard, S., P. B. Christensen and L. P. Nielsen. 1995. Seasonal variation in nitrification and denitrification in estuarine sediment colonized by benthic microalgae and bioturbating infauna. Mar. Ecol. Progr. Ser., *126,* 111–121.

Sayama, M. and Y. Kurihara. 1983. Relationship between burrowing activity of the polychaetous annelid, *Neanthes Japonica* (Izuka) and nitrification-denitrification processes in the sediments. J. Expl. Mar. Biol. Ecol., *72,* 233–241.

Seitzinger, S. P. 1988. Denitrification in freshwater and coastal marine ecosystems: ecological and geochemical significance. Limnol. Oceanogr., *33,* 702–724.

Seitzinger, S. P. and A. E. Giblin. 1996. Estimating denitrification in North Atlantic continental shelf sediments. Biogeochemistry, *35,* 235–260.

Strickland, J. D. H. and T. R. Parsons. 1972. A practical handbook of sea water analysis. Bull. Fish. Res. Board Can., *169,* 1–311.

Thamdrup, B. and T. Dalsgaard. 2000. The fate of ammonium in anoxic manganese oxide-rich marine sediment. Geochim. Cosmochim. Acta, *64,* 4157–4164.

Tiedje, J. M., S. Sinkins and P. M. Groffman. 1989. Perspectives on measurement of denitrification in the fields including recommended protocols for acetylene based methods. Plant. Soil, *115,* 261–284.

Ullman, W. J. and R. C. Aller. 1982. Diffusion coefficients in nearshore marine sediments. Limnol. Oceanogr., *27,* 552–556.

Van Cappellen, P., J.-F. Gaillard and C. Rabouille. 1993. Biogeochemical transformation in sediments: kinetic models of early diagenesis, *in* Interactions of C, N, P and S Biogeochemical Cycles and Global Change, R. Wollast, F. T. Mackenzie and L. Chou, eds., NATO ASI Series, 401–445.

Van Cappellen, P. and Y. Wang. 1996. Cycling of iron and manganese in surface sediments: a general theory for the coupled transport and reaction of Carbon, Oxygen, Nitrogen, Sulfur, Iron and Manganese. Am. J. Sci., *296,* 197–243.

Vanderborght, J. and G. Billen. 1975. Vertical distribution of nitrate concentration in interstitial water of marine sediments with nitrification and denitrification. Limnol. Oceanogr., *20,* 953–961.

Woodin, S. A. and R. Marinelli. 1991. Biogenic habitat modification in marine sediments: the importance of species composition and activity, *in* The Environmental Impact of Burrowing Animals and Animal Burrows, P. S. Meadows and A. Meadows, eds., A. Zool. Soc. London Symposia, *63,* 231–250.